Introduction

This document provides additional results, more details on the calculations of the models and physico-chemical properties of the compounds and solutions used by some of the models.

S1 Additional results

The following sections contain a comparison of the predictions between myristic acid and sodium myristate (NaC14) for models in which we had the necessary information to perform the calculations, namely the simple partitioning, compressed film, and partial organic film models. In addition, a sensitivity analysis of the compressed film model is provided with respect to the organic molar volume. A more comprehensive sensitivity analysis is available in the Supplement of Vepsäläinen et al. (2022). The comparison and the sensitivity analysis are provided here because due to a lack of available parameters, we used the compressed model specific parameters ($A_0, m_\sigma, \log C_0$ and $\sigma_{\min}$) created for myristic acid in calculations with NaC14. The comparison and sensitivity analysis may help to understand how large the uncertainty created by these parameters is.

In addition, a comparison between the predictions of the partial organic film model when a constant minimum surface thickness is used and when the surface thickness given by the monolayer model is used is included below.

For myristic acid, the properties of the pure compound used during model calculations are: molar mass M = 228.371 $\mathrm{g\,mol^{-1}}$, liquid phase density $\rho_\mathrm{l} = 882.2725\ \mathrm{kg\,m^{-3}}$ (Noureddini et al., 1992), solid phase density $\rho_\mathrm{s} = 862.2$ (at 54 °C) $\mathrm{kg\,m^{-3}}$ (CRC Handbook, 1988) and the pure compound surface tension $\sigma = 32.0584\ \mathrm{mN\,m^{-1}}$ (the method of Zhang et al. (2018), using data from Di Nicola et al. (2016)).

S1.1 Myristic acid and NaC14 comparison

Figures S1 and S2 contain the Köhler curves and droplet surface tensions along the Köhler curves predicted with the simple partitioning, compressed film, and partial organic film models for myristic acid (continuous lines) and NaC14 (dashed lines) for initial dry particle size of D_p = 50 nm at surfactant mass fractions ($w_\mathrm{p,sft}$) of 0.2, 0.5, 0.8 and 0.95 in the dry particles. Table S1 contains the droplet diameters, supersaturations, and surface tensions at the critical point of cloud droplet activation predicted with the three models corresponding to Figs. S1 and S2. A constant value of 0.5 nm was used for the minimum surface thickness (δ) with the partial organic film calculations. The same compressed film model parameters (A_0, m_σ, C_0) were used for both compounds during the calculations of the compressed film model. For the calculation of water activity, a dissociation factor of two was used for NaC14 and a factor of one for pure acid.

Figure S1 shows that the differences in the predictions between pure myristic acid NaC14 are consistent, preserving the shape of the Köhler curves with the different models. The particles containing myristic acid have a higher predicted $\mathrm{SS_c}$ and a smaller d_c (Tables S1, S2 and S3). The predictions of the compressed film model show a maximum increase of 15% in $\mathrm{SS_c}$ and a maximum of 13% decrease in d_c for $w_\mathrm{p,sft} = 0.8$ when the particles contain myristic acid instead of NaC14. The predictions of the simple partitioning model show an increase of 15 % for $\mathrm{SS_c}$ and a decrease of 12 % in d_c for the same conditions. The maximum difference between myristic acid and NaC14 for the predictions of the partial organic model is greater, the d_c of the acid is smaller by a maximum of 65 %, and the supersaturation is greater than with NaC14 by a maximum of 33 %, both at $w_\mathrm{p,sft}$ = 0.95. This considerably larger change in d_c is a result of the critical point moving to a droplet size where the organic surface film has not yet broken (Fig. S1(d)). This is a consequence of the higher surface tension of pure myristic acid than that of the value at the CMC for binary water-NaC14 used for the calculations with NaC14 in the absence of the pure compound surface tension.

Figure S2 shows the droplet surface tensions along the Köhler curves predicted with the different models. The simple partitioning model always assumes a surface tension equal to that of water. The predictions of the compressed film model are similar for both compounds, but the point where the surface tension of water is reached changes due to different organic molar volumes, as the sensitivity analysis shows (Fig. S4). The surface tension predicted with the partial organic film model shifts with the surface film breaking at different droplet sizes and the lower limit of the surface tension represented by the horizontal dashed black lines is different but the shape of the curve remains similar. The lower limit for the surface tension for droplets containing NaC14 is the binary NaC14-water surface tension at the CMC while for myristic acid, the lower surface tension is

Table S1. The critical droplet diameters (d_c), supersaturations (SS_c) and surface tensions (σ_c) for the different models for simulations with particles containing myristic acid and NaC14 at 298.15 K for D_p = 50 nm. The partial organic film calculations were performed at a constant minimum surface thickness $\delta = 0.5$ nm.

Parameter	d_c (nm)	SS_c (%)	σ_c (mN m^{-1})	d_c (nm)	SS_c (%)	σ_c (mN m^{-1})	d_c (nm)	SS_c (%)	σ_c (mN m^{-1})
	Myristic acid								
$w_{p,sft}$	Simple			Compressed film			Partial organic film		
0.2	367.33	0.38	71.97	391.33	0.36	71.97	399.29	0.35	68.15
0.5	251.26	0.56	71.97	267.67	0.53	71.97	333.1	0.42	61.54
0.8	146.71	0.98	71.97	154.95	0.92	71.97	285.99	0.49	53.86
0.95	84.68	1.84	71.97	116.54	1.57	71.97	110.66	0.59	32.06
	NaC14								
$w_{p,sft}$	Simple			Compressed film			Partial organic film		
0.2	389.09	0.36	71.97	414.51	0.34	71.97	424.16	0.33	68.11
0.5	281.09	0.5	71.97	298.6	0.47	71.97	373.72	0.37	61.44
0.8	167.47	0.85	71.97	177.39	0.8	71.97	333.1	0.42	53.78
0.95	93.38	1.63	71.97	130.76	1.38	71.97	315.38	0.44	49.49

Table S2. The absolute differences in critical droplet diameters (d_c), supersaturations (SS_c) and surface tensions (σ_c) for the different models for simulations between myristic acid and NaC14 (Δ = myristic acid - NaC14 predictions) at 298.15 K for D_p = 50 nm. The partial organic film calculations were performed at a constant minimum surface thickness $\delta = 0.5$ nm.

Parameter	Δd_c (nm)	ΔSS_c (%)	$\Delta\sigma_c$ (mN m^{-1})	Δd_c (nm)	ΔSS_c (%)	$\Delta\sigma_c$ (mN m^{-1})	Δd_c (nm) (nm)	ΔSS_c (%)	$\Delta\sigma_c$ (mN m^{-1})
$w_{p,sft}$	Simple			Compressed film			Partial organic film		
0.2	-21.76	0.02	0	-23.18	0.02	0	-24.87	0.02	0.04
0.5	-29.84	0.06	0	-30.93	0.06	0	-40.63	0.05	0.1
0.8	-20.76	0.13	0	-22.44	0.12	0	-47.11	0.07	0.08
0.95	-8.7	0.21	0	-14.21	0.19	0	-204.71	0.15	-17.44

that of the pure compound (Zhang et al., 2018; Di Nicola et al., 2016). Tables S2 and S3 show that the droplet surface tension at activation is the same or near the same value for both systems in Figs. S2(a)-S2(c). In Fig. S2(d), the shift in the critical droplet diameter also leads to considerably lower droplet surface tension, all the way to the lower limit due to the organic surface film still being intact, with the particles containing myristic acid.

S1.2 Compressed film model sensitivity to organic molar volume

Figures S3 and S4 show the predictions of Köhler curves and the droplet surface tension during droplet growth with the compressed film model for particles containing myristic acid with variable molar volume and a single curve for particles containing NaC14, both mixed with NaCl. The same model parameters from Forestieri et al. (2018) have been used for both myristic acid and NaC14. The parameters were originally fitted for myristic acid. A more detailed analysis of the compressed model sensitivity was previously provided in the Supplement of Vepsäläinen et al. (2022).

Fig. S3 shows that varying the organic molar volume only affects the Köhler curves at higher surfactant mass fractions in the particles (Figs. S3(c) and (d) with $w_{p,sft} = 0.8$ and 0.95, respectively) and is more focused on the smaller droplet sizes. The critical point is only significantly affected in Fig. S3(d). In Fig. S3(d), the predicted critical point of the droplets containing

Table S3. The ratios of critical droplet diameters (d_c), supersaturations (SS_c) and surface tensions (σ_c) for the predictions of the different models between myristic acid and NaC14 at 298.15 K for D_p = 50 nm. The partial organic film calculations were performed with a constant $\delta = 0.5$ nm.

Parameter	$\frac{d_c^{acid}}{d_c^{NaC14}}$	$\frac{SS_c^{acid}}{SS_c^{NaC14}}$	$\frac{\sigma_c^{acid}}{\sigma_c^{NaC14}}$	$\frac{d_c^{acid}}{d_c^{NaC14}}$	$\frac{SS_c^{acid}}{SS_c^{NaC14}}$	$\frac{\sigma_c^{acid}}{\sigma_c^{NaC14}}$	$\frac{d_c^{acid}}{d_c^{NaC14}}$	$\frac{SS_c^{acid}}{SS_c^{NaC14}}$	$\frac{\sigma_c^{acid}}{\sigma_c^{NaC14}}$
$w_{p,sft}$	Simple			Compressed film			Partial organic film		
0.2	0.94	1.06	1.0	0.94	1.06	1.0	0.94	1.06	1.0
0.5	0.89	1.12	1.0	0.9	1.12	1.0	0.89	1.12	1.0
0.8	0.88	1.15	1.0	0.87	1.15	1.0	0.86	1.17	1.0
0.95	0.91	1.13	1.0	0.89	1.14	1.0	0.35	1.33	0.65

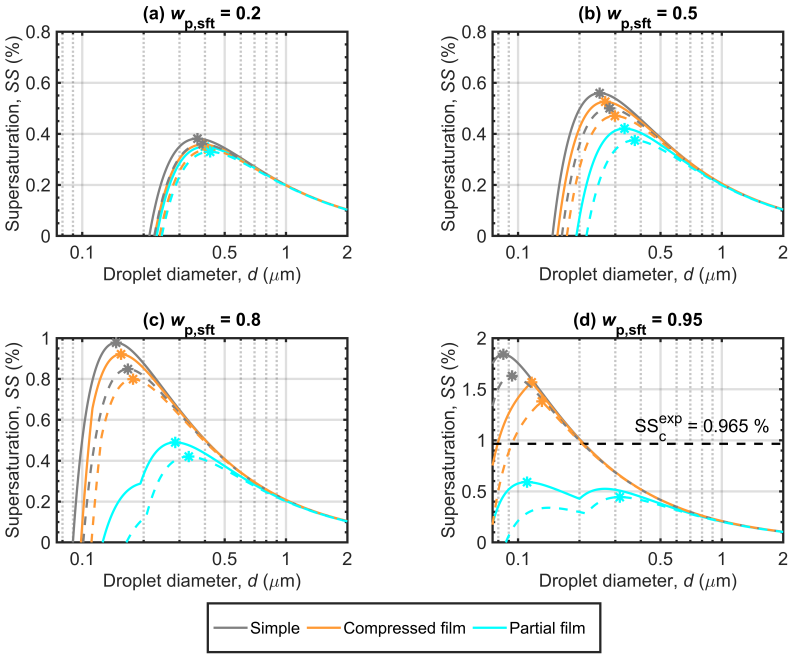

Figure S1. The Köhler curves predicted with the simple partitioning, compressed film, and partial organic film models at different surfactant mass fractions ($w_{p,sft}$) in particles at $D_p = 50$ nm containing myristic acid (continuous lines) and NaC14 (dashed lines), both mixed with NaCl. The critical points are also marked. Note that the vertical axis scaling changes between the panels.

NaC14 is in the shaded red area, denoting different levels of variation in the myristic acid molar volume. The predicted intersection corresponds to a rough decrease of about 30 % in the molar volume of myristic acid. Calculated with the molar masses and solid phase densities given in Table 1 of the main article, the myristic acid molar volume is about 27 % larger than that of NaC14, which is in good agreement with Fig. S3(d). The shape of the Köhler curve between myristic acid and NaC14 is similar, but the shape of the curve from variations in the molar volume of myristic acid is not fully in agreement with the shape of the NaC14 curve.

Figure S4 shows how the predicted surface tension curve remains the same shape with varying molar volume, but the point where the surface tension value of water is reached and the rising part of the curve leading to it are shifted as a function of the droplet size. The curves predicted with particles containing myristic acid and NaC14 are of similar shape.

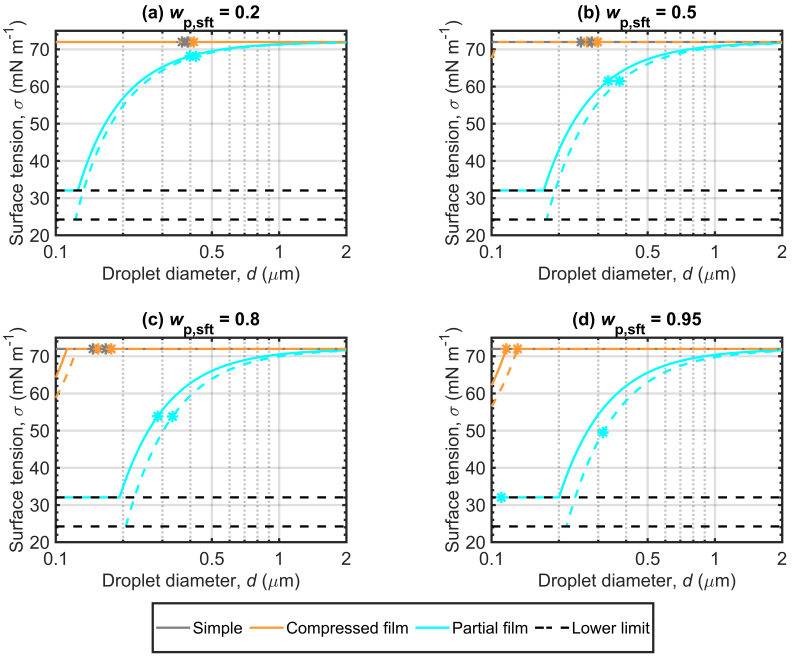

Figure S2. Surface tensions along the Köhler curves modeled with the simple partitioning, compressed film and partial organic film models at different surfactant mass fractions ($w_{\mathrm{p,sft}}$) in the particles for myristic acid (continuous lines) and NaC14 (dashed lines). The critical points are also marked. The lower limit for the surface tension (marked in the legend as "Lower limit") for droplets containing NaC14 is the surface tension of the binary NaC14-water mixture at the CMC, while for myristic acid, the lower limit is that of the pure compound (Zhang et al., 2018; Di Nicola et al., 2016).

S1.3 Partial organic film model constant δ

Figure S5 shows the supersaturation predicted with the monolayer and partial organic film models for $D_{\mathrm{p}} = 50$ nm and at surfactant mass fractions ($w_{\mathrm{p,sft}}$) of 0.2, 0.5, 0.8 and 0.95. The partial organic film model calculations were performed at the minimum surface layer thickness equal to that calculated by the monolayer model (δ_{ML}) and with a constant surface thickness of 0.5 nm ($\delta_{0.5}$). The δ values calculated with the monolayer model for NaC14 are between 0.39 and 0.88 nm, depending on the droplet size (smaller droplets have a larger surface thickness). The mean surface thickness values are 0.44, 0.44, 0.45, 0.45 nm for $w_{\mathrm{p,sft}} = 0.2, 0.5, 0.8$ and 0.95 respectively. Fig. S5 shows that the main effect of the different minimum surface film thickness is a minor one for the critical point. The $\mathrm{SS_c}$ is slightly higher with constant surface thickness in all panels of Fig. S5, while d_{c} is slightly smaller in Figs. S5(a) and (b) and slightly larger in Figs. S5(c) and (d). Using the constant surface thickness makes the breaking of the organic film visible for Figs. S5 (c) and (d), while the monolayer calculations could not be performed at all small droplet sizes (and therefore no surface thickness value was available to perform calculations with for these droplet sizes).

Figure S6 contains the droplet surface tensions along the Köhler curves predicted with the monolayer and partial organic film models for $D_{\mathrm{p}} = 50$ nm and at surfactant mass fractions ($w_{\mathrm{p,sft}}$) of 0.2, 0.5, 0.8 and 0.95. Again, the partial organic film model calculations were performed with the monolayer surface thickness and a constant surface thickness, as detailed in the previous paragraph. Similarly to the Köhler curves, the main difference between the two partial organic film model predictions is at smaller droplet sizes, where the constant surface thickness leads to the organic surface film breaking at larger particle sizes. Furthermore, the overall shape of the predicted surface tension curve is slightly different with the constant surface thickness, but only to a small degree.

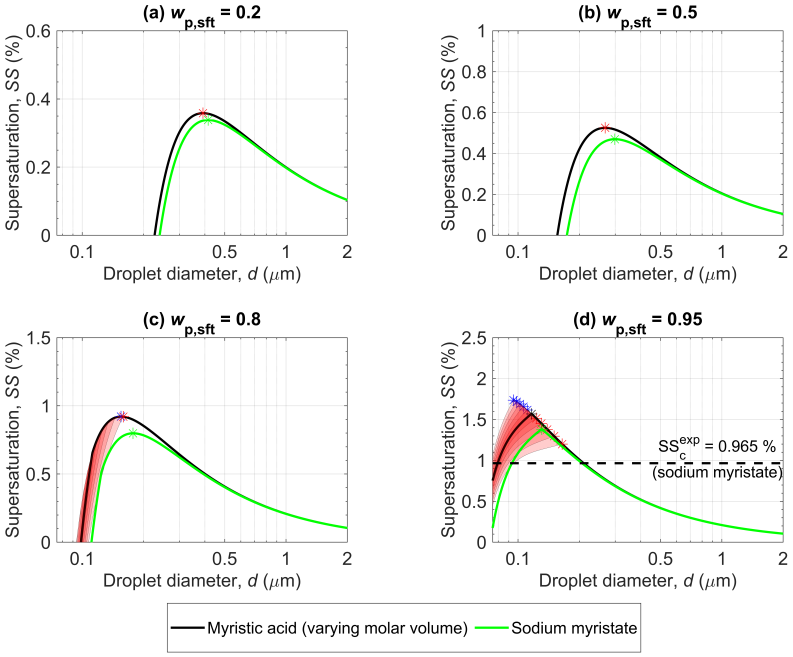

Figure S3. Supersaturation predicted with the compressed film model at different surfactant mass fractions ($w_{\mathrm{p,sft}}$) for myristic acid (black line) with varying organic molar volume visible as the shaded red areas corresponding to $\Delta\% = \pm 10\%, \pm 20\%, \pm 30, \pm 40\%$ and $\pm 50\%$ variations. The variation is calculated as $\bar{v} \cdot X$ where X is the multiplier taken as $(100\% \pm \Delta\%)/100$. The critical points predicted with positive changes in molar mass are marked in blue, and the critical points predicted with negative changes are marked in red. Additionally, the predictions for NaC14-NaCl particles (green line) are visible, as is $\mathrm{SS_c^{exp}}$ from Prisle et al. (2008) in panel (d) for pure NaC14. Note that the vertical axis scaling changes between the panels.

Table S4 contains the critical droplet properties as well as the absolute differences and the ratios between the predicted critical droplet properties for the partial organic film model calculations performed with a surface thickness equal to that of the monolayer model or with a constant surface thickness of 0.5 nm. The calculation of the difference was performed as $\delta_{\mathrm{ML}} - \delta_{0.5}$. The d_{c} has a shift of 24.47 nm at maximum for $w_{\mathrm{p,sft}} = 0.95$ between the predictions. The $\mathrm{SS_c}$ is always higher in predictions with constant surface thickness, though only by 0.016 % at most for $w_{\mathrm{p,sft}} = 0.8$. Surface tension at the point of cloud droplet activation is also always higher with constant surface thickness, at most by 4.4 $\mathrm{mN,\ m^{-1}}$ for $w_{\mathrm{p,sft}} = 0.95$.

S2 Calculation details

The following sections contain details related to the calculation of water activity, droplet surface tension, and droplet solution density. Details for the calculation of initial amounts of salt, surfactant, and water in the droplets, as well as water activity calculations that have not been detailed below, can be found in the Supplement of Vepsäläinen et al. (2022).

S2.1 Water activity

The water activity in ternary droplet solutions is calculated as the corrected mole fraction, with both NaCl and NaC14 having a dissociation factor of two. A dissociation factor of one has been used for myristic acid calculations.

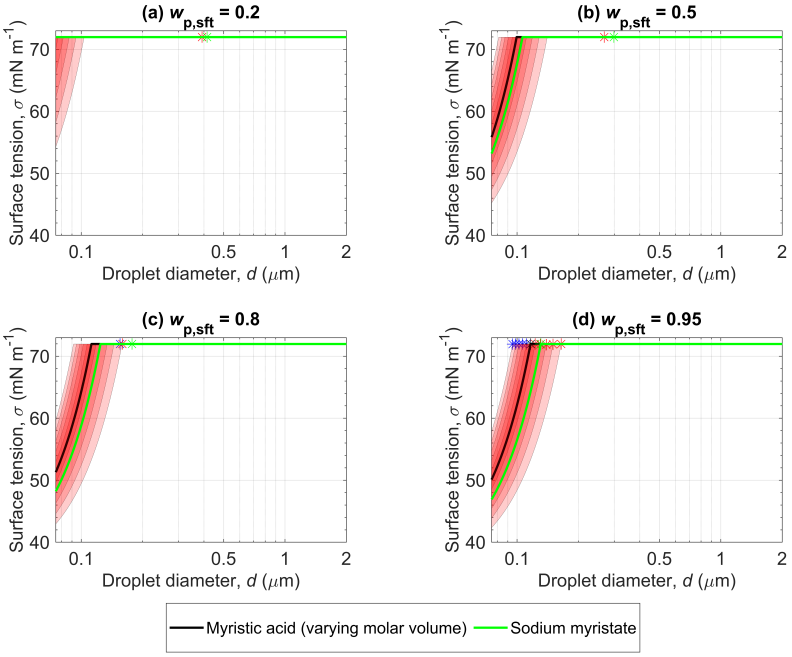

Figure S4. Surface tensions along the Köhler curve predicted with the compressed film model at different surfactant mass fractions ($w_{\mathrm{p,sft}}$) for myristic acid-NaCl particles (black line) with varying organic molar volume (red shaded areas corresponding to $\Delta\% = \pm10\%, \pm20\%, \pm30, \pm40\%$ and $\pm50\%$ variations). The variation is calculated as $\bar{v}\cdot X$ where X is the multiplier taken as $(100\% \pm \Delta\%)/100$. The critical points predicted with positive changes in molar mass are marked in blue, and the critical points predicted with negative changes are marked in red. Furthermore, the surface tensions along the Köhler curves predicted for NaC14-NaCl particles (green line) are visible in the different panels of the figure above.

The AIOMFAC-based (AIOMFAC-web, 2022) water activity fit used for the simple partitioning model (Prisle et al., 2011) and the partial organic film model (Ovadnevaite et al., 2017) is

$$a_{\mathrm{w}} = (113.8753 \cdot x_{\mathrm{salt}}^2 + 83.4706 \cdot x_{\mathrm{salt}} + 35.5768) \cdot \exp(-10.2524 \cdot x_{\mathrm{salt}}) - 34.5768 \cdot \exp(-8.0822 \cdot x_{\mathrm{salt}}), \quad \text{(S1)}$$

where x_{salt} is the mole fraction of the salt (sodium chloride). The fit was created at 298.15K for a mole fraction range of $x_{\mathrm{salt}} = 10^{-7} - 0.26$.

S2.2 Surface tension

The surface tension of pure NaC14 is extended from the binary fit, and therefore the value is that of the surface tension at the CMC. Surface tension of pure NaCl is calculated according to the equation given by Vanhanen et al. (2008) that originates from Janz (1980). The binary surface tension of water and NaC14 was determined from Wen et al. (2000) though data digitized by using the *WebPlotDigitizer* (Rohatgi, 2021). The fit was made at 298.15 K and follows the form of the Szyszkowski–Langmuir equation (Szyszkowski, 1908) given in Prisle et al. (2008). The fit equation (in N m^{-1}) is

$$\sigma = \sigma_{\mathrm{w}} - 0.007042 \ln(1 + 2.81 \cdot 10^7 \cdot \min(x, x_{\mathrm{CMC}})), \quad \text{(S2)}$$

where σ_{w} is the surface tension of water (IAPWS, 2014), x is the mole fraction of NaC14 and x_{CMC} is the critical micelle concentration as a mole fraction.

Table S4. The critical droplet diameters (d_c), supersaturations (SS_c) and surface tensions (σ_c) for partial organic film model simulations with surface thickness equal to the output of the monolayer model (δ_{ML} and a constant $\delta = 0.5$ nm ($\delta_{0.5}$). The table also displays the absolute differences in the predicted critical properties between the two simulations, and ratios of the two critical properties. The absolute difference has been calculated as predictions with $\delta_{ML} - \delta_{0.5}$. The fraction between the different critical properties is calculated as $\delta_{ML}/\delta_{0.5}$.

Parameter	d_c (nm)	SS_c (%)	σ_c (mN m^{-1})	d_c (nm)	SS_c (%)	σ_c (mN m^{-1})
$w_{p,sft}$	Partial organic film (δ_{ML})			Partial organic film ($\delta_{0.5}$)		
0.2	432.19	0.32	67.27	423.73	0.33	68.1
0.5	382.52	0.36	60.03	373.44	0.37	61.43
0.8	328.87	0.4	51.51	332.95	0.42	53.77
0.95	291.05	0.43	45.11	315.52	0.44	49.51
	$\delta_{ML} - \delta_{0.5}$			$\delta_{ML}/\delta_{0.5}$		
$w_{p,sft}$	Δd_c (nm)	ΔSS_c (%)	$\Delta\sigma_c$ (mNm^{-1})	$\frac{d_{c,ML}}{d_{c,0.5}}$	$\frac{SS_{c,ML}}{SS_{c,0.5}}$	$\frac{\sigma_{c,ML}}{\sigma_{c,0.5}}$
0.2	8.46	-0.0068	-0.83	1.02	0.98	0.99
0.5	9.07	-0.015	-1.4	1.02	0.96	0.98
0.8	-4.09	-0.016	-2.26	0.99	0.96	0.96
0.95	-24.47	-0.0095	-4.4	0.92	0.98	0.91

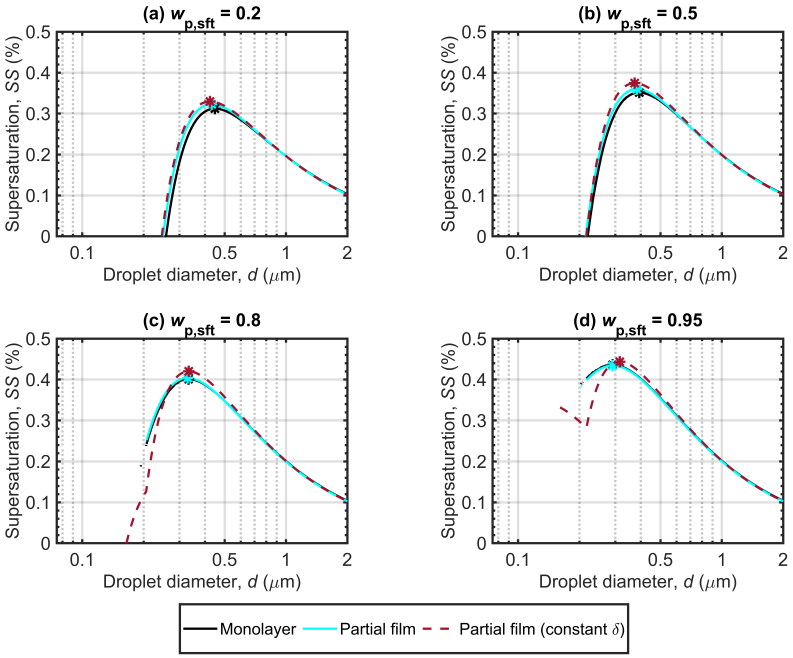

Figure S5. The Köhler curves modeled with the monolayer and partial organic film models for $D_p = 50$ nm at different surfactant mass fractions ($w_{p,sft}$) of 0.2, 0.5, 0.8, and 0.95. The critical points are also marked.

The ternary surface tension of water, NaC14 and NaCl was also fitted to the digitized (Rohatgi, 2021) data of Wen et al. (2000) using the form of the Szyszkowski–Langmuir equation Szyszkowski (1908) given by Prisle et al. (2010). The fitting

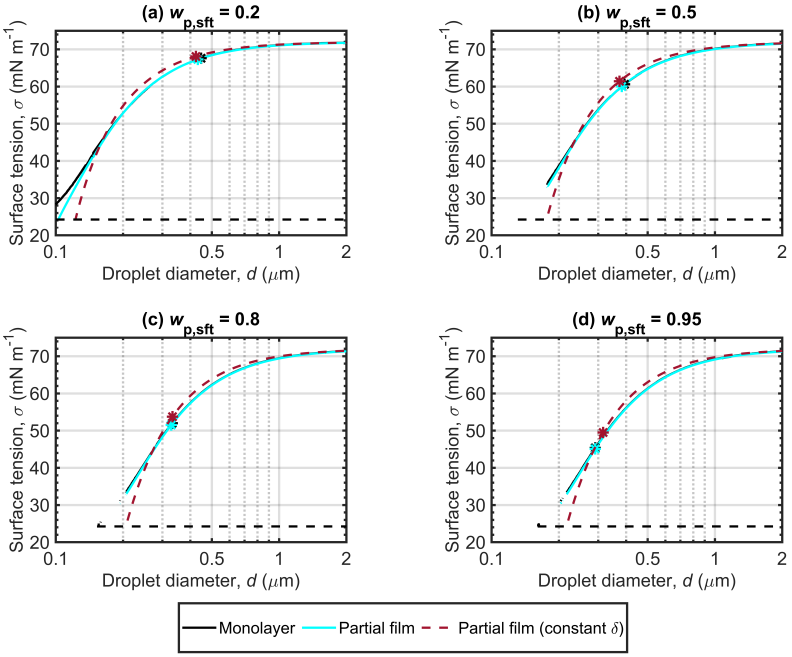

Figure S6. The droplet surface tensions along the Köhler curves modeled with the monolayer and partial organic film models for $D_{\mathrm{p}} = 50$ nm at different surfactant mass fractions ($w_{\mathrm{p,sft}}$) of 0.2, 0.5, 0.8, and 0.95. The critical points are also marked, as well as the lower surface tension limit of the droplet (the surface tension at the CMC).

Table S5. Fitting parameters for Eqs. (S4) and (S4).

i	1	2	3
a_i	15.4246	-2.9546	-4.5712
b_i	$0.0776 \cdot 10^{-4}$	$0.3776 \cdot 10^{-4}$	$-0.4262 \cdot 10^{-4}$

equation is

$$\sigma = \sigma_{\mathrm{w}} + \left(\frac{d\sigma_{\mathrm{NaCl}}}{dm_{\mathrm{NaCl}}}\right) m_{\mathrm{NaCl}} - a \ln(1 + m_{\mathrm{sft}}/b) \tag{S3}$$

where

$$a = a_1 + a_2 w_{\mathrm{sft}} + a_3 w_{\mathrm{sft}}^2, \tag{S4}$$

$$b = b_1 + b_2 w_{\mathrm{sft}} + b_3 w_{\mathrm{sft}}^2, \tag{S5}$$

and m is the molality of NaCl or surfactant depending on the index. The parameters for Eqs. (S4) and (S5) can be found in Table S5. Eq. (S3) gives the surface tension in units of $\mathrm{mN\ m^{-1}}$ with the given parameters and therefore σ_{w} needs to be in the same units. The salt gradient (Vanhanen et al., 2008; Prisle et al., 2010) in Eq. (S3) is

$$\frac{d\sigma_{\mathrm{NaCl}}}{dm_{\mathrm{NaCl}}} = 1.61(\mathrm{mN\ m^{-1}})/(\mathrm{mol\ kg^{-1}}).$$

The maximum possible surface tension given by the fit is limited by the maximum amount of salt soluble in water. The solubility of NaCl in water was adjusted to the data of Pinho and Macedo (2005). The fitted equation for the solubility in terms of NaCl mass fraction is

$$w_{\mathrm{sol,NaCl}} = (0.0001374T^2 - 0.06899T + 34.84) \cdot 10^{-2}. \tag{S6}$$

The maximum possible surface tension of the ternary solution is set at the solubility limit as the binary surface tension of water saturated with NaCl as given by the fit of Vanhanen et al. (2008). The surface tension of the ternary solution cannot be lower than the pure surfactant or, in this case, the surface tension at the CMC for the binary solution of water and NaC14. In addition, boundary conditions have been added that constrain the ternary fit at the pure compound as well as the binary surface tensions of water–salt and water–organic salt mixtures at the corresponding compositions.

Pure surface tension of myristic acid is calculated using the method of Zhang et al. (2018) with initial data from Di Nicola et al. (2016).

S2.3 Density

The density of pure liquid NaC14 is extended from the density of binary solution of water and NaC14. The binary aqueous density is estimated using the method of Calderón and Prisle (2021), as is the ternary density of water, NaC14 and NaCl. According to the method, the density of binary aqueous surfactant solutions is calculated using the apparent molal volume of the surfactant Φ_{sft} as

$$\rho = \frac{1 + m_{\mathrm{sft}} M_{\mathrm{sft}}}{1/\rho_{\mathrm{w}} + 1 \cdot 10^{-6} \Phi_{\mathrm{sft}} m_{\mathrm{sft}}} \tag{S7}$$

where m_{sft} and M_{sft} are the molality and the molar mass of the surfactant, respectively, and ρ_{w} is the density of pure water (Pátek et al., 2009). The apparent partial molal volume of the surfactant changes due to micellization and its value can be calculated as

$$\Phi_{\mathrm{sft}} = H\left(\mathrm{CMC} - m_{\mathrm{sft}}\right)\left(\Phi_{\mathrm{sft}}^{\infty} + A_v\sqrt{m_{\mathrm{sft}}} + B_{\mathrm{sft}}^{V} m_{\mathrm{sft}}\right) + H\left(m_{\mathrm{sft}} - \mathrm{CMC}\right)\left(\xi\Phi_{\mathrm{sft}}^{\mathrm{CMC}} + (1-\xi)V_{\mathrm{mic}}\right), \tag{S8}$$

where CMC is in molal units, $\Phi_{\mathrm{sft}}^{\infty}$ and $\Phi_{\mathrm{sft}}^{\mathrm{CMC}}$ are the apparent molal volume of the surfactant at infinite dilution and at the CMC in $\mathrm{cm}^3\,\mathrm{mol}^{-1}$, respectively, and H is the Heaviside step function. In addition, the fraction of micellization ξ is estimated from a concentration-dependent parametrization of the CMC as a function of the salt molality (Lisi et al., 1980)

$$\xi = \left(\frac{(\mathrm{sgn}\left(m_{\mathrm{sft}} - \mathrm{CMC}\right) + 1)}{2}\right)\frac{m_{\mathrm{sft}} - \mathrm{CMC}}{m_{\mathrm{sft}}} \tag{S9}$$

The model parameter B_{sft}^{V} is used to include the effect of surfactant-surfactant interactions with consistent units of $\mathrm{cm}^3\,\mathrm{mol}^{-2}\,\mathrm{kg}$. These model parameters have been obtained from Vikingstad et al. (1978) and Blanco et al. (2005) for NaC14 or a similar compound if direct data was not available.

The partial molar volumes at $25°\mathrm{C}$ are from Vikingstad et al. (1978). At infinite dilution $\Phi_{\mathrm{sft}}^{\infty} = 226.4\ \mathrm{cm}^{-3}\,\mathrm{mol}^{-1}$and at the CMC $\Phi_{\mathrm{sft}}^{\mathrm{CMC}} = 226.5\,\mathrm{cm}^{-3}\,\mathrm{mol}^{-1}$.

In the absence of data for NaC14, a B_{sft}^{V} parametrization for sodium dodecanoate was used based on Blanco et al. (2005) as

$$B_{\mathrm{sft}}^{V} = -35.26\exp\left(-\left(\frac{(T-317.3)}{7.893}\right)^2\right) + 90.18\exp\left(-\left(\frac{(T-301.6)}{47.41}\right)^2\right) \tag{S10}$$

The variable V_{Mic} is the surfactant molal volume in micellar form. Its value depends on the change in molar volume experienced by the surfactant during micellization as

$$V_{\mathrm{mic}} = \Phi_{\mathrm{sft}}^{\mathrm{CMC}} + \Delta V_{\mathrm{mic}}. \tag{S11}$$

The $\Delta V_{\rm mic}$ is a temperature-dependent parameter that here we have taken at 25°C from Vikingstad et al. (1978): $\Delta V_{\rm mic} = 14.3$ $\rm cm^3 mol^{-1}$.

The variable A_v represents the Debye-Hückel limiting slope in volume units, $\left(\rm cm^3\ kg^{1/2}\ mol^{-3/2}\right)$ calculated as

$$A_v = 1.50619 + 0.0130073(T-273.15) + 4.8307\times10^{-5}(T-273.15)^2 + 8.95087\times10^{-7}(T-273.15)^3 \\ -3.727\times10^{-9}(T-273.15)^4 + 2.3942\times10^{-11}(T-273.15)^5 \tag{S12}$$

according to Millero (2014). Eqs. (S7)-(S12) are used to estimate the density of aqueous NaC14.

The ternary density of the solution of water, NaC14 and NaCl is estimated using a pseudo- binary approach that uses the mean apparent molal volume ($\bar{\Phi}$) of the solutes from the mixing rule of Young and Smith (1954)

$$\bar{\Phi} = \frac{m_{\rm sft}\Phi_{\rm sft} + m_{\rm NaCl}\Phi_{\rm NaCl}}{m_{\rm sft} + m_{\rm NaCl}} \tag{S13}$$

The density of the ternary solution is calculated as

$$\rho = \frac{1 + m_{\rm sft}M_{\rm sft} + m_{\rm NaCl}M_{\rm NaCl}}{1/\rho_w + (m_{\rm sft} + m_{\rm NaCl})\bar{\Phi}\cdot10^{-6}}. \tag{S14}$$

The apparent molal volume of the surfactant is calculated with equation (S8). However, now the presence of salt affects micellization and therefore the parameters of Eq (S8). The fraction of counterions associated with micelles in aqueous solutions was not available for NaC14, and therefore a value reported by Vikingstad et al. (1978) for aqueous sodium dodecanoate was used $\beta_0 = 0.74$. The effect of NaCl (ternary solution) according to Calderón and Prisle (2021) can be accounted for with

$$\beta = \beta_0 + 2.2297 m_{\rm NaCl}. \tag{S15}$$

For the ternary solution, the effect of the inorganic salt on the volume change during micellization $\Delta V^{\rm ter}_{\rm mic}$ is defined via equation

$$\Delta V^{\rm ter}_{\rm mic} = (\Delta V_{\rm mic} - 4.681\beta_0) - 23.35 m_{\rm NaCl} + 4.681\beta \tag{S16}$$

and then

$$V_{\rm mic} = \Phi^{\rm CMC}_{\rm sft} + \Delta V^{\rm ter}_{\rm mic}. \tag{S17}$$

The apparent partial molal volume of the salt is calculated according to the model of Rogers and Pitzer (1982) as

$$\Phi_{\rm NaCl} = \Phi^{\infty}_{\rm NaCl} + 2A_v\frac{\ln(1+b\sqrt{I})}{2b} + 2RT\left(m_{\rm NaCl}B^V_{\rm NaCl} + m^2_{\rm NaCl}C^V_{\rm NaCl}\right), \tag{S18}$$

where $\Phi_{\rm NaCl}$ and $\Phi^{\infty}_{\rm NaCl}$ are the apparent partial molal volume of NaCl in the solution and at a hypothetical infinite dilute solution, I is the ionic strength of the solution defined as $I = 0.5\sum z_i^2 m_i$, where z_i is the ion valence; b is a model parameter equal to 1.2 $\rm kg^{0.5}\ mol^{-0.5}$ equal for all electrolyte systems. The value of A_v is calculated via equation (S12).

Calderón and Prisle (2021) presents the following equations for calculating the parameters $\Phi^{\infty}_{\rm NaCl}$, $B^v_{\rm NaCl}$ and $C^v_{\rm NaCl}$:

$$\Phi^{\infty}_{\rm NaCl} = -0.001462T^2 + 0.9609T - 139.9, \tag{S19}$$

$$B^v_{\rm NaCl} = 0.2694\exp(-0.03379T) + 2.611\times10^{-8}\exp(0.01245\cdot T) \text{ and} \tag{S20}$$

$$C^v_{\rm NaCl} = -0.04196\exp(-0.03719T). \tag{S21}$$

Eqs.(S19)–(S21) have been acquired by fitting temperature-dependent models of each parameter to the experimental densities of NaCl solutions ($T = 273-373$ K and p= 1 bar) presented by Pitzer et al. (1984). Both the binary and ternary densities of the water–surfactant or water–surfactant–salt solutions are constrained by the pure compound densities.

Pure density of liquid myristic acid is calculated from Noureddini et al. (1992).

$$\rho = (-6.727 \cdot 10^{-4} \cdot (T - 273.15) + 8.9909 \cdot 10^{-1}) \cdot 1000 \tag{S22}$$

Pure density of liquid NaCl is calculated using an extrapolation (in the temperature range) of Janz (1980). The binary density of water and NaCl is estimated as explained in Calderón and Prisle (2021), using the model of Pitzer (1955):

$$\rho = \left(\frac{m_{\mathrm{NaCl}} \cdot \Phi_{\mathrm{NaCl}} + 1000 \cdot V_1^{\circ}/M_{\mathrm{w}})}{1000 + m_{\mathrm{NaCl}} M_{\mathrm{NaCl}}} \right)^{-1} \cdot 1000 \tag{S23}$$

where

$$V_1^{\circ} = 42.8 \exp(-0.01254T) + 12.6 \exp(0.001014T) \tag{S24}$$

is a temperature-dependent relationship fitted to experimental data for this variable. For the details, see the Supplement of Calderón and Prisle (2021). The molal volume of salt Φ_{NaCl} is calculated with Eq. (S18).

S2.4 Critical micelle concentration

The calculations of the present work employ the critical micelle concentration of a binary mixture of water and NaC14. The value was specifically determined from the digitized (by employing Rohatgi (2021)) measurements of Wen et al. (2000), the same data set used for the ternary surface tension fit. This was done to ensure internal consistency of the simulations and to avoid any unrealistic values as well as sudden step-increases or decreases in the surface tension fits themselves.

The CMC value was determined directly as a mole fraction of the surfactant from a $(\ln(x_{\mathrm{sft}}), \sigma)$ plot via fitting of two straight lines, one to the linearly decreasing surface tension and one to the baseline of minimal surface tension. The intersection point of the two lines is taken as the CMC value. Determined in this way, $x_{\mathrm{CMC}} = 3.1191 \cdot 10^{-5}$ with the corresponding surface tension being $\sigma_{\mathrm{CMC}} = 24.2483\ \mathrm{mNm}^{-1}$.

S2.5 NaC14 $\mathrm{SS}_{\mathrm{c}}^{\mathrm{exp}}$

Prisle et al. (2008) measured experimental critical supersaturations as a function of dry particle diameter, and fitted the results as power functions. The equation given for NaC14 is

$$y = 271.74 \cdot x^{-1.4417}, \tag{S25}$$

where y denotes the $\mathrm{SS_c}$ and x the dry particle size. For $D_{\mathrm{p}} = 50$ nm, Eq. (S25) gives $\mathrm{SS}_{\mathrm{c}}^{\mathrm{exp}} = 0.9655\%$.

References

AIOMFAC-web: version 3.03, https://aiomfac.lab.mcgill.ca, accessed: 2022-08-1, 2022.

Blanco, E., González-Pérez, A., Ruso, Juan, M., Pedrido, R., Prieto, G., and Sarmiento, F.: A comparative study of the physicochemical properties of perfluorinated and hydrogenated amphiphiles, J. Colloid Interface Sci., 288, 247–260, https://doi.org/https://doi.org/10.1016/j.jcis.2005.02.085, 2005.

Calderón, S. M. and Prisle, N. L.: Composition dependent density of ternary aqueous solutions of ionic surfactants and salts, J. Atmos. Chem, 78, 99–123, https://doi.org/10.1007/s10874-020-09411-8, 2021.

CRC Handbook: CRC Handbook of Chemistry and Physics, 1st Student Edition, edited by Weast, R. C. , CRC Press, Boca Raton, FL., 1988.

Di Nicola, G., Coccia, G., and Pierantozzi, M.: A new equation for the surface tension of carboxylic acids, Fluid Phase Equilib., 417, 229 – 236, https://doi.org/https://doi.org/10.1016/j.fluid.2016.03.001, 2016.

Forestieri, S. D., Staudt, S. M., Kuborn, T. M., Faber, K., Ruehl, C. R., Bertram, T. H., and Cappa, C. D.: Establishing the impact of model surfactants on cloud condensation nuclei activity of sea spray aerosol mimics, Atmos. Chem. Phys., 18, 10 985–11 005, https://doi.org/10.5194/acp-18-10985-2018, 2018.

International Association for the Properties of Water and Steam (IAPWS): Revised Release on Surface Tension of Ordinary Water Substance: IAPWS R1-76 (2014), Moscow, http://www.iapws.org/relguide/Surf-H2O.html, last access: 18.3.2020, 2014.

Janz, G. J.: Molten Salts Data as Reference Standards for Density, Surface Tension, Viscosity, and Electrical Conductance: KNO3 and NaCl, J. Phys. Chem. Ref. Data, 9, 791–830, https://doi.org/10.1063/1.555634, 1980.

Lisi, R. D., Perron, G., and Desnoyers, J. E.: Volumetric and thermochemical properties of ionic surfactants: sodium decanoate and octylamine hydrobromide in water, Can. J. Chem., 58, 959–969, https://doi.org/10.1139/v80-152, 1980.

Millero, F.: Estimation of the Partial Molar Volumes of Ions in Mixed Electrolyte Solutions Using the Pitzer Equations, J. Solution Chem., 43, 1448–1465, https://doi.org/10.1007/s10953-014-0213-0, 2014.

Noureddini, H., Teoh, B. C., and Davis Clements, L.: Densities of vegetable oils and fatty acids, J. Am. Oil Chem. Soc., 69, 1184–1188, https://doi.org/10.1007/BF02637677, 1992.

Ovadnevaite, J., Zuend, A., Laaksonen, A., Sanchez, K. J., Roberts, G., Ceburnis, D., Decesari, S., Rinaldi, M., Hodas, N., Facchini, M. C., Seinfeld, J. H., and O'Dowd, C.: Surface tension prevails over solute effect in organic-influenced cloud droplet activation, Nature, 546, 637–641, https://doi.org/10.1038/nature22806, 2017.

Pinho, S. P. and Macedo, E. A.: Solubility of NaCl, NaBr, and KCl in Water, Methanol, Ethanol, and Their Mixed Solvents, J. Chem. Eng. Data, 50, 29–32, https://doi.org/10.1021/je049922y, 2005.

Pitzer, K. S.: The Volumetric and Thermodynamic Properties of Fluids. I. Theoretical Basis and Virial Coefficients1, J. Am. Chem. Soc., 77, 3427–3433, https://doi.org/10.1021/ja01618a001, 1955.

Pitzer, K. S., Peiper, J. C., and Busey, R. H.: Thermodynamic Properties of Aqueous Sodium Chloride Solutions, J. Phys. Chem. Ref. Data, 13, 1–102, https://doi.org/10.1063/1.555709, 1984.

Prisle, N. L., Raatikainen, T., Sorjamaa, R., Svenningsson, B., Laaksonen, A., and Bilde, M.: Surfactant partitioning in cloud droplet activation: a study of C8, C10, C12 and C14 normal fatty acid sodium salts, Tellus B, 60, 416–431, https://doi.org/10.1111/j.1600-0889.2008.00352.x, 2008.

Prisle, N. L., Raatikainen, T., Laaksonen, A., and Bilde, M.: Surfactants in cloud droplet activation: mixed organic-inorganic particles, Atmos. Chem. Phys., 10, 5663–5683, https://doi.org/10.5194/acp-10-5663-2010, 2010.

Prisle, N. L., Dal Maso, M., and Kokkola, H.: A simple representation of surface active organic aerosol in cloud droplet formation, Atmos. Chem. Phys., 11, 4073–4083, https://doi.org/10.5194/acp-11-4073-2011, 2011.

Pátek, J., Hrubý, J., Klomfar, J., Součková, M., and Harvey, A. H.: Reference Correlations for Thermophysical Properties of Liquid Water at 0.1 MPa, J. Phys. Chem. Ref. Data, 38, 21–29, https://doi.org/10.1063/1.3043575, 2009.

Rogers, P. S. Z. and Pitzer, K. S.: Volumetric Properties of Aqueous Sodium Chloride Solutions, J. Phys. Chem. Ref. Data, 11, 15–81, https://doi.org/10.1063/1.555660, 1982.

Rohatgi, A.: Webplotdigitizer: Version 4.5, https://automeris.io/WebPlotDigitizer, accessed: 2021-10-1 – 2021-10-12, 2021.

Szyszkowski, B.: Experimentelle Studien über kapillare Eigenschaften der wässerigen Lösungen von Fettsäuren., Zeitschrift für Physikalische Chemie, 64U, 385–414, https://doi.org/doi:10.1515/zpch-1908-6425, 1908.

Vanhanen, J., Hyvärinen, A.-P., Anttila, T., Raatikainen, T., Viisanen, Y., and Lihavainen, H.: Ternary solution of sodium chloride, succinic acid and water; surface tension and its influence on cloud droplet activation, Atmos. Chem. Phys., 8, 4595–4604, https://doi.org/10.5194/acp-8-4595-2008, 2008.

Vepsäläinen, S., Calderón, S. M., Malila, J., and Prisle, N. L.: Comparison of six approaches to predicting droplet activation of surface active aerosol – Part 1: moderately surface active organics, Atmos. Chem. Phys., 22, 2669–2687, https://doi.org/10.5194/acp-22-2669-2022, 2022.

Vikingstad, E., Skauge, A., and Høiland, H.: Partial molal volumes and compressibilities of the homologous series of sodium alkylcarboxylates, R6COONa–R13COONa, in aqueous solution, J. Colloid Interface Sci., 66, 240–246, https://doi.org/10.1016/0021-9797(78)90301-6, 1978.

Wen, X., Lauterbach, J., and Franses, E. I.: Surface Densities of Adsorbed Layers of Aqueous Sodium Myristate Inferred from Surface Tension and Infrared Reflection Absorption Spectroscopy, Langmuir, 16, 6987–6994, https://doi.org/10.1021/la991326s, 2000.

Young, T. F. and Smith, M. B.: Thermodynamic Properties of Mixtures of Electrolytes in Aqueous Solutions, J. Phys. Chem., 58, 716–724, https://doi.org/10.1021/j150519a009, 1954.

Zhang, C., Tian, J., Zheng, M., Yi, H., Zhang, L., and Liu, S.: A new corresponding state-based correlation for the surface tension of organic fatty acids, Mod. Phys. Lett. B, 32, 1750 361, https://doi.org/10.1142/S0217984917503614, 2018.